Contract No.:

This manuscript has been authored by Savannah River Nuclear Solutions (SRNS), LLC under Contract No. DE-AC09-08SR22470 with the U.S. Department of Energy (DOE) Office of Environmental Management (EM).

Disclaimer:

Raman Signatures from Age-Dating PuO_2 Since Last Calcination

Eliel Villa-Aleman*, Amanda L. Houk, Thomas C. Shehee and Nicholas J. Bridges

Savannah River National Laboratory
Aiken, SC 29808 United States

*Corresponding Author: eliel.villa-aleman@srnl.doe.gov

Abstract
The self-irradiation of PuO_2 has been shown to affect the attributes of fifteen vibrational bands in the Raman spectrum. The vibrational bands correspond to the Raman allowed vibrational mode T_{2g}, overtones, defects, and bands from electronic origin. Defects in the crystal lattice from low-calcination temperature and alpha decay origins are responsible for the changes in the band attributes (band position, full-width half maximum (FWHM), intensity). Crystal lattice defects are also responsible for the growth of the defect bands. The temporal behavior of the vibrational bands can be used to estimate the age of the material since last calcination. Laser annealing was used to reset the material to full crystallinity prior to the aging study. $^{240}PuO_2$, with an alpha decay rate of 3.67 greater than the decay rate of $^{239}PuO_2$, was primarily used to assess the alpha decay-induced damage within 3 years. The aging study focused on the time-dependent properties of the T_{2g} band and the growth of defect bands. The FWHM of the T_{2g} band and the ratio of the areas of the defect bands/T_{2g} band were measured through a time period in excess of 3 years. The data from this study were found very close to the data describing the temporal evolution of the lattice constant measured with the X-ray diffraction (XRD) technique. The local physical properties of the material measured with Raman spectroscopy and the lattice parameter constant measured with XRD indicates a strong correlation between the two techniques. Although both techniques provide similar age-dating information, in contrast to the few milligram quantities required for XRD, Raman spectroscopy requires a 10 μm diameter PuO_2 particle to provide an estimate of the material age since last calcination.

Keywords: plutonium dioxide, alpha decay, age-dating, lattice damage, laser annealing, nuclear forensics

Introduction
PuO_2 belongs to the fluorite structure group which is described as a face centered cubic sublattice. Group theory analysis of PuO_2 results in one Raman active mode, the T_{2g} mode, located near 480 cm^{-1}, and two infrared active modes located near 270 and 580 cm^{-1} (infrared reflectivity measurements) [1]. The creation of cation and anion Frenkel pairs via alpha decay can lead to structural changes within the crystal and a change in the crystal symmetry. PuO_2 properties are sensitive to: 1) initial production conditions (calcination temperature), 2) crystal lattice damage via self-irradiation and 3) environmental effect via water absorption with subsequent hydrogen production and the oxidation of Pu to other values besides +IV [1-4].

The preparation of the PuO_2 at different temperatures and from different precursors ($Pu(NO_3)_2$, PuF_4, $PuCl_4$, Pu oxalate, Pu metal, etc.) produce materials with different particle size and crystallinity which in turn affects the vibrational spectral properties [3]. The precursors used in the production of the PuO_2 material can template the morphology of the particulates. The different calcination temperatures affect the crystallinity of the material and therefore the band structure due to lattice defects [5]. Low calcination temperatures result in defects in the crystal lattice or smaller particulates with amorphous properties. As calcination temperature increases, coalescence of nanoparticles results in longer range crystallinity.

The degree of crystallinity is slowly altered over time by the plutonium alpha decay as indicated by the expansion of the lattice constant measured with X-ray diffraction (XRD) [6]. The energetic alpha particles and recoiling nuclei create significant, detectable defects and vacancies in the crystal

structure [3, 4, 6]. Raman microspectroscopy can detect these changes over time by interrogating PuO_2 localized physical properties [3, 4]. Several defect Raman bands (up to four) have been observed in the PuO_2 Raman spectrum with age [3, 7]. In the defect band cluster region, two main bands (near 580 cm^{-1} and 650 cm^{-1}) overwhelm the defect spectral region. The defect bands suggest that a change in the crystal lattice symmetry and possibly other defects in the crystal lattice such as vacancies and substitutional defects, are responsible for the new defect bands in the Raman spectrum.

The expansion of the lattice constant ($\frac{\Delta a}{a_0}$, where Δa is the change in lattice parameter via self-radiation and a_0 is the lattice parameter after preparation) in an actinide material of the O_h^5 point group has been shown to depend on the cumulative alpha-irradiation dose [6, 8-15]. The lattice expansion of actinide oxides, such as $^{238}PuO_2$, $^{239}PuO_2$, $^{241}AmO_2$ and $^{243}CmO_2$ has been studied by several groups [8-13]. Kato *et al.* used the lattice constant expansion to study the self-radiation damage in plutonium and uranium mixed dioxide materials with different Pu concentrations and storage time [6]. The lattice constant expansion and rate of change is related to the isotope ratios and the half-life of the isotopes in the sample. The function describing the expansion of the lattice parameter is shown in equation 1 where A and B are constants and τ is the decay constant of the actinide metal.

$$\frac{\Delta a}{a_0} = A(1 - e^{-B\tau t}) \qquad (1)$$

Materials not properly calcined and/or annealed show an expansion in the crystal lattice. Typical calcination temperatures in the production of PuO_2 from Pu-bearing compounds are 723, 923 and 1273 K. The calcination of Pu-bearing precursors at 723 K is used to destroy organics. Calcination at higher temperatures (923 K) reduces the surface area of the material [5]. Meanwhile, calcination at temperatures >1173 K results in a PuO_2 material with ceramic-like properties [5]. Most of PuO_2 research is conducted with low-temperature calcined materials for enhanced material solubility [1, 16-22]. Since PuO_2 can absorb water up to 2% w/w of the material, the resultant hydrogen production results in a potential explosive atmosphere. High-fired PuO_2 is used for long-term storage due to the ceramic-like properties. Spectroscopic analysis of PuO_2 must consider the high variability of calcination temperatures, surface area and the possibility of material degradation to assess calcination temperature and age.

Water absorption by PuO_2 can create an explosive environment via the generation of H_2. Los Alamos National Laboratory (LANL) reported a chemical reaction between PuO_2 and water in the 323 to 623 K temperature range according to the equation $PuO_2(s) + x\ H_2O \rightarrow PuO_{2+x}(s) + H_2(g)$ where x assumes a value up to 2.25 [23]. LANL also indicated that the addition of oxygen into the lattice results in the generation of mixed valence state containing Pu^{+4} and Pu^{+5} [23]. Pu_4O_9 and/or Pu_4O_8-OH chemical formulas were postulated to maintain charge neutrality between Pu and O in the primitive cell level. A small lattice constant expansion was observed during the water/PuO_2 chemical reaction. Although the changes in the crystal lattice and the formation of Pu^{+5} had been observed with extended X-ray absorption fine structure (XAFS) and X-ray photoelectron spectroscopy (XPS), no definite vibrational band assignment for the plutonyl-like material had been made [23]. Bands at 745 and 833 cm^{-1} corresponding to the $(O = Pu^{+5} = O)^+$ and the $(O = Pu^{+6} = O)^{2+}$, respectively, and have been identified in aqueous solutions [1, 24]. Most likely, we have not

identified similar vibrational modes in solid media since our material has not been exposed to water vapor to induce alternate Pu oxidations. In the uranium system, the Raman spectrum of U_4O_9 was measured by Desgranges *et al.* and the defect band (D_2) near 580 cm^{-1} was assigned as U_4O_9 [25]. It is possible that the band located at 650 cm^{-1} corresponds to Pu_4O_9.

The auto-irradiation of the PuO_2 material, in contrast to PuO_2 reaction with water, results in an exponential change of the crystal lattice expansion that plateaus with time depending on the lifetime of the isotope. The PuO_2 reaction with water and the alpha decay auto-irradiation are clearly two different and independent mechanisms. Calcination temperature and alpha decay determines the population and type of crystal lattice defects in the material. Higher the calcination temperature, smaller the defect population in the material. Therefore, significant reduction of defects is observed for high-fired PuO_2 (>1173 K) relative to the defect population for the PuO_2 calcined at 723 K.

Alpha decay induces significant damage to the crystal lattice resulting in the production of different defects. Wolfer *et al.* calculated $3x10^9$ alpha events per gram per second for ^{239}Pu resulting in a displacement rate of roughly 0.1 displacements per atom (dpa) per year [2]. Schwartz et al. calculated that 90% of the Frenkel pairs returns to their original site leaving behind about 10% as free interstitials and vacancies or clusters of both [26]. A 5 MeV alpha particle travels approximately 10 μm in the crystal with approximately 265 Frenkel pairs occur near the end of the range [2]. Meanwhile, the 86 keV ^{235}U recoil nucleus has a range of 12 nm and creates roughly 2300 Frenkel pairs. The alpha particle and the uranium atom recoil bores a tunnel in the crystal lattice. The tunnel consists of a low atomic density in the center with a high density of interstitial atoms along the walls. The high concentration of defects (anion and cation Frenkel pairs) created along the walls of the tunnel gives rise to a Raman spectrum with new bands assigned to defects and changes in the band attributes. Significant damage to the position of the atoms in the crystal results in changes in the bonding structure of the material.

Besides calcination and irradiation borne defects, the introduction of dopants in the material can enhance the intensity of the defect bands. Nakajima *et al.* studied the formation of defects in the CeO_2 material with Y_2O_3, La_2O_3 and ZrO_2 doping [27]. Two bands in the defect region were identified as D_{1D} and D_2. The D_2 band was assigned to a defect with O_h symmetry that includes a dopant cation in 8-fold coordination of O^{2-}. Meanwhile, the D_1 defect include an O^{2-} vacancy with symmetry different from that of the O_h^5 point group.

Taniguchi *et al.* studied the defects in gadolinia (Gd_2O_3) doped CeO_2 with UV resonance Raman spectroscopy [28]. Taniguchi *et al.* proposed two different types of complexes to explain the Gd dopant with O^{2-} vacancies in a non-O_h symmetry structure $(2Gd'_{Ce}:V_{O^{\cdot\cdot}})^x$ and $(Gd'_{Ce}:V_{O^{\cdot\cdot}})^*$ [28]. Their data also supports that the shift of the D_1 band is accompanied by the increase of the $(2Gd'_{Ce}:V_{O^{\cdot\cdot}})^x$ from $(Gd'_{Ce}:V_{O^{\cdot\cdot}})^*$ [28]. Charge neutrality in the complexes assumes 2 Gd^{3+} atoms with two oxygen vacancies. The band ratio for the defect/T_{2g} for undoped CeO_2 calcined at different temperatures reduced significantly for high temperature annealing. Little changes were observed for the CeO_2 with the Gd^{3+} dopants for different annealing temperatures.

Longitudinal and transverse optical modes observed in Raman and infrared spectroscopy are dependent on the symmetry of the crystal. Symmetry relaxation in disordered crystals or a change in the metal oxidation and new bonds introduce additional fundamental modes. Distortion of the

atomic structure in the crystal results in changes in the intensity, FWHM and position of the bands. The changes in the intensities of the vibrational modes are related to the population, polarizability, resonance effects, and the phonon-electron interactions. The line broadening in a system is related to the Heisenberg uncertainty, $\Delta E \Delta t \geq \hbar$, where Δt is the lifetime of the system (phonon lifetime) and ΔE is the uncertainty in the energy. The phonon lifetime depends on the decay to other phonons and scattering by defects. The Raman line shape, Γ, is controlled by the phonon dephasing time, T_2; $\Gamma = (\pi c T_2)^{-1}$. The phonon dephasing time, T_2, has contributions from the pure dephasing time (τ_{ph}), and phonon population lifetime (T_1). For systems where inhomogeneous broadening is negligible, T_2, T_1 and τ_{ph}, are related through the equation: $2/T_2 = 1/\tau_{ph} + 1/T_1$. Only when the pure dephasing time is large, the phonon dephasing time can be equated to the phonon population lifetime. Band position is related to the force constants holding the atoms in their position. Defects in the crystal induces a weakening of the bonds holding the lattice together.

To understand the band structure in a Raman spectrum and to extract meaningful information from the age of the material, a clear understanding of the parameters affecting the band attributes is required. Band attributes are primarily affected from: 1) experimental conditions of the Raman measurements which could lead to material heating and instant laser annealing, 2) synthesis conditions of the PuO_2 and 3) age of the material. It is the goal of this work to show how the band properties and the new defect bands emerging in the Raman spectrum can be used to date the material age since last calcination. The new age-dating methodology can be used in the characterization of several PuO_2 isotopes calcined at different temperatures. This research will show that the shape of the age-dating curve acquired with Raman spectroscopy is similar to the expansion of the lattice constant curve acquired with XRD.

Materials and Methods

The methodology for producing the plutonium (^{240}Pu) material has been discussed previously [3, 4] and briefly discussed here. Plutonium (^{240}Pu and ^{239}Pu) material was synthesized within a once-through, multiple HEPA filtered, negative pressure glovebox. The plutonium material used plutonium holdings at Savannah River National Laboratory. The plutonium material was dissolved in nitric acid (HNO_3) and purified using an anion exchange (Relliex HPQ) followed by elution in 0.35 M HNO_3. PuO_2 was produced by calcining the eluted solution in air at 723, 923 and 1273 K (450, 650 and 1000°C) for two hours. The prepared samples were stored and sealed in a double wall containment cell [3] under ambient conditions in air.

The Raman microscope system has been described previously [3, 4, 29]. Briefly, Raman spectra of PuO_2 were measured with a modified commercial system (LabRAM HR800 UV, Horiba Jobin-Yvon) along with a Newton EMCCD (Andor 970N-UVB) detector, accurate within 0.5 cm^{-1}. LabSpec 5.78 software controlled the spectrometer and detector. The detector was calibrated to account for any intensity nonlinearities across the visible and near-infrared region of the detector. A 514 nm laser line from an Ar ion laser measured the PuO_2 Raman spectra with powers <5mW at the sample. The laser wavelength plays an important role in the ratio of the T_{2g} band to the other bands in the spectrum and in the intensity of the defect bands. At long wavelengths (>632 nm), the T_{2g} band significantly overwhelms the other bands in the PuO_2 spectrum. At wavelengths shorter than 632 nm, the intensity of the overtone, defects, and electronic bands begin to increase in intensity relative to the T_{2g} band. A significant amount of visible laser light is absorbed by the PuO_2 material. The laser power on the sample can induce heating depending on the size of the

particulates which then results in band intensity, position and FWHM changes. The conditions used in these experiments ensures that the attributes of the bands were not affected during the measurements.

Five different crystalline particle aggregates (150-300 μm diameter, composed of nm size crystals) within the $^{240}PuO_2$ sample calcined at 1273 K were annealed with 50 mW of power for ten minutes with a 514 nm excitation laser using a 50x microscope objective to anneal an area of approximately 6 μm in diameter at the particle aggregate surface. Measurements were also taken on non-laser annealed spots on the same five different crystalline particle aggregates to collect spectra at later times since last calcination (>380 days). There is overlap of laser annealed and non-laser annealed spectra data from 380 to 550 days. Neutral density filters controlled the laser intensity at the sample.

Age of the material accounts for the variability in the vibrational band attributes. As the material ages, new bands emerge in the spectrum. Environmental and/or alpha decay can induce changes in the spectral properties. In the case of uranium, oxidation can lead to chemical changes where UO_2 can become U_3O_8, U_4O_9, etc. PuO_2 has been found to undergo further oxidation in the presence of water which could lead to the production of Pu_4O_9 and/or Pu_4O_8-OH. Alpha decay of the material induces most of the changes observed in the band properties related to the age of the material. In this work the rate of the observed band changes has been correlated with isotopic content and decay rate [4].

Results and Discussion

The fluorite structure group of PuO_2 is described as a face centered cubic (fcc) sublattice (O_h^5 point group) [1, 3, 4]. The symmetry group predicts a triply degenerate Raman active T_{2g} mode, and the T_{1u} TO IR mode and the non-degenerate T_{1u} LO IR. The IR bands for the PuO_2 isostructural compounds have been very difficult to characterize using absorption spectroscopy. The IR reflection spectroscopy technique using Kramers-Kronig relationship, has been used to characterize the IR bands for CeO_2, UO_2, ThO_2 and PuO_2 [30, 31]. Hyper-Raman spectroscopy was used by Villa-Aleman *et al.* to record the T_{1u} TO and the non-degenerate T_{1u} LO mode of CeO_2 IR bands with high sensitivity [29]. The hyper-Raman spectrum of ThO_2, although not published, was also recorded while conducting CeO_2 research suggesting that in the future, hyper-Raman spectroscopy might be used to characterize the IR bands of PuO_2.

The Raman spectra of PuO_2 calcined at different temperatures are significantly more complex than the single active Raman band near 480 cm^{-1} predicted from group symmetry. Figure 1 shows the 10-spot averaged $^{240}PuO_2$ Raman spectra for samples calcined at 723, 923 and 1273 K. The spectra were acquired with the 514 nm laser line from an Ar ion laser and normalized to the T_{2g} band. Since the $^{240}PuO_2$ samples were analyzed approximately 3 months after its synthesis, the spectra show the composite behavior of incomplete calcination (crystallinity) and aging effects. Since the PuO_2 sample calcined at 1273 K is mostly crystalline, emerging defect bands are primarily the result of material aging. Similar band structure was observed for the PuO_2 spectra calcined at different temperatures. The main differences are observed in the FWHM of the bands and the intensity of the defect bands. Since calcination temperature correlates with the crystal lattice structure, the higher the calcination temperature, the sharper the bands and smaller the intensity of the defect bands.

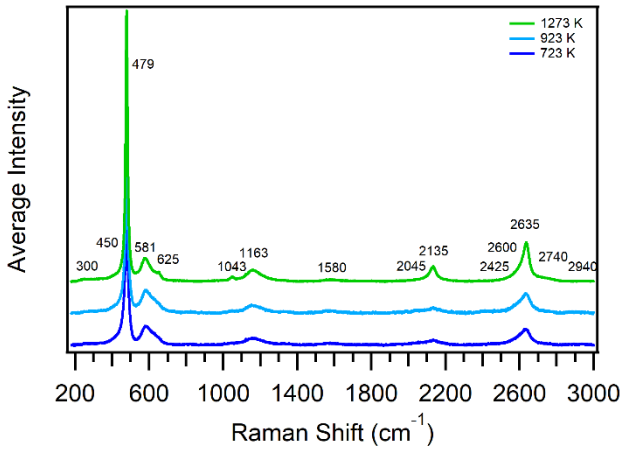

Fig. 1. Raman spectra of $^{240}PuO_2$ samples calcined at 1273, 923 and 723 K (green, light blue and dark blue spectra, respectively) excited with 514 nm laser light. Spectra are averages of 10 different spots on each sample, normalized to the T_{2g} band at 479 cm^{-1} and offset to show bands for each calcination condition.

Band Structure

Five dominant Raman bands are present in the PuO_2 spectrum at 479, 581, 1163, 2135 and 2635 cm^{-1} and ten additional PuO_2 Raman bands are consistently observed in the spectra in Figure 1 at 300, 450, 625, 1043, 1580, 2045, 2425, 2600, 2740 and 2940 cm^{-1}. As the sample ages, new bands emerge in the spectrum while other bands disappear and most bands shift. The T_{2g} mode (1LO1) located near 479 cm^{-1} is the only Raman allowed transition. The band located at 581 cm^{-1} (defect band) is the 1LO2 mode which is an IR active band. The 1163 cm^{-1} band is attributed to an overtone band of the 1LO2 mode (i.e., 2LO2). The bands located at 2135 and 2635 cm^{-1} are identified as electronic bands. The assignment of many of these bands is based on Raman and infrared work conducted with CeO_2, UO_2, ThO_2, and NpO_2, and hyper-spectra of CeO_2 and ThO_2 [1, 3, 4, 29-31]. Table 1 lists the assignments for the five dominant Raman bands in Figure 1.

Table 1. PuO_2 Raman band assignments.

Band Position (cm^{-1})	Assignment	Band Origin
479	T_{2g} (1LO1)	Vibrational
581	1LO2	Vibrational
1163	2LO2	Vibrational
2135	$\Gamma_1 \rightarrow \Gamma_5$	Electronic
2635	$\Gamma_1 \rightarrow \Gamma_3$	Electronic

All the bands in the spectra (five dominant and ten additional PuO_2 Raman bands were consistently observed in samples prepared from different Pu-bearing precursors, such as plutonium oxalates, fluorides and nitrate and under different experimental conditions (different excitation wavelengths, focusing conditions and integration times). The exact location of the bands (usually within a few wavenumbers) is dependent on intrinsic and experimental parameters used in the analysis. The material crystallinity, laser power used during the analysis and the impurities in the material are the most important parameters affecting the band location. Lorentzian fits and deconvolution software

were used to identify the exact spectral position in broad bands, such as the 581 and 625 cm^{-1} bands in the 1LO2 region. Lorentzian lineshapes have been used previously to analyze similar oxides [32-34]. The 300 cm^{-1} band has been identified as the T_{1u}, the 450 cm^{-1} could be interpreted as the T_{2g} shape evolution due to confinement and inhomogeneous strain effects due to particle size distribution or an overtone of the T_{2g} band, the 1043 cm^{-1} has been identified as an electronic band by our group, the 2045 cm^{-1} as a crystal effect on the electronic band of the 2135 cm^{-1} and the 2425, 2600, 2740 and 2940 cm^{-1} as satellite bands to the 2635 cm^{-1} band. The 1580 cm^{-1} band might be attributed to carbon impurities during the calcination of the PuO_2 material.

Primary Bands in the Alpha Decay Study

Although most of the vibrational bands in Figure 1 can be used to estimate the age of the material, this study concentrated on the bands located in the 250 to 750 cm^{-1} spectral region. Temporal information can be obtained from changes in the band attributes. The band position, the FWHM of the T_{2g} band, the areas of the ratios of the T_{2g} band and two defect bands (581 and 625 cm^{-1}) and the areas of the ratio of the areas of the 581 cm^{-1} and the 625 cm^{-1} bands can be used to provide an estimate of the age of the material since last calcination. Figure 2 shows the Raman spectra of a laser-annealed PuO_2 sample at different times over a period of two and a half years within the 250 to the 750 cm^{-1} range. The temporal changes in the bands' structure are evident in the spectra. In order to simplify the age-dating discussion and compare the evolution of the bands, band A refers to the T_{2g} band, band B refers to the T_{1u} band located at 581 cm^{-1} and band C to the band located in the 625 to 650 cm^{-1} range, as shown in Figure 3. It is worthwhile to point out that four bands have been identified in the defect band region. Also, as the material ages, the 625 cm^{-1} is overwhelmed by a band at 650 cm^{-1}. Nakajima *et al.* and Taniguchi *et al.* working with doped CeO_2 coined bands B and C to the D_1 and D_2 defects, respectively [27, 28]. Figure 3 shows the spectrum including the defect band region with each band labeled and fit with a Lorentzian.

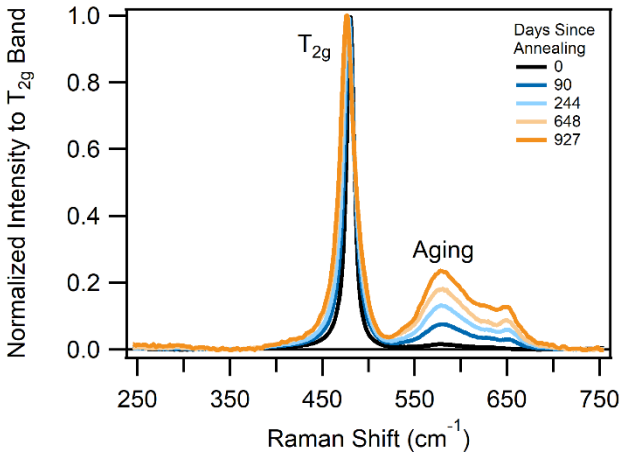

Fig. 2. Normalized Raman spectra of $^{240}PuO_2$ after annealing and aged under ambient conditions for over 2.5 years collected with 514 nm laser light.

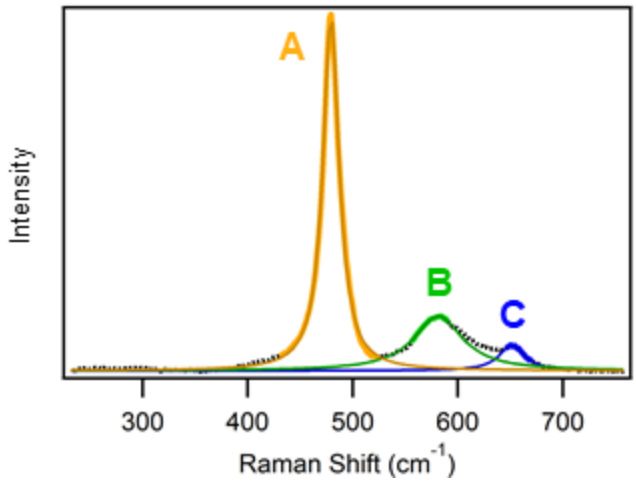

Fig. 3. Example Raman spectrum of $^{240}PuO_2$ sample with each band fit with a Lorentzian. Band A (orange line) is the T_{2g} band near 480 cm^{-1}, band B (green line) is the 1LO2 band near 580 cm^{-1} and band C (blue line) is an additional aging band near 650 cm^{-1}.

The broadening of the band corresponding to the T_{2g}, A, vibrational mode and growth of the two bands, B and C, are attributed to defects in the crystal lattice from alpha-induced crystal lattice defects or low-temperature synthesis of the material, which may not have annealed all defects in the material. Schoenes [35] proposed that the band B is related to the T_{1u} 1LO2 band observed in the infrared spectrum due to a change in symmetry due to crystal lattice damage while Taniguchi et al. [28] have proposed a complex of metal (M^{3+}) and O^{2-} vacancies. In either case, the O^{2-} vacancies might be responsible for the loss of symmetry and the observation of the IR band in the Raman spectrum. Band C (625 cm^{-1}, the band becomes 650 cm^{-1} with age) does not have an analogue in the infrared spectrum. The defect bands in this region studied with gadolinium-induced doping by Taniguchi et al. suggest a metal ion in the center of the O^{2-} cube [28]. In general, the bands B and C are identified as anion and cation Frankel pairs. We have identified up to four defect bands in this spectral region [3]. The intensity of these bands is highly dependent on the laser wavelength used in the Raman measurement. Longer wavelengths (561, 633, and 733 nm) reduces band B intensity while increasing band C intensity while shorter laser wavelengths increase the band B relative to bands A, and C [3].

Figure 4 shows the data curves corresponding to the FWHM of A, and the B/A, C/A and C/B ratios of the areas from the laser-annealed $^{240}PuO_2$ sample originally calcined at 1273 K. Each point in the curve represents the average of five spots (10 μm diameter) of previously laser-annealed material. As mentioned previously, the FWHM is related to the phonon dephasing time, T_2 via the equation $\Gamma = (\pi c T_2)^{-1}$. Since the dephasing time is related to the phonon population time (T_1) through the equation $2/T_2 = 1/\tau_{ph} + 1/T_1$, for a large pure dephasing time (τ_{ph}), $2/T_2 = 1/T_1$.

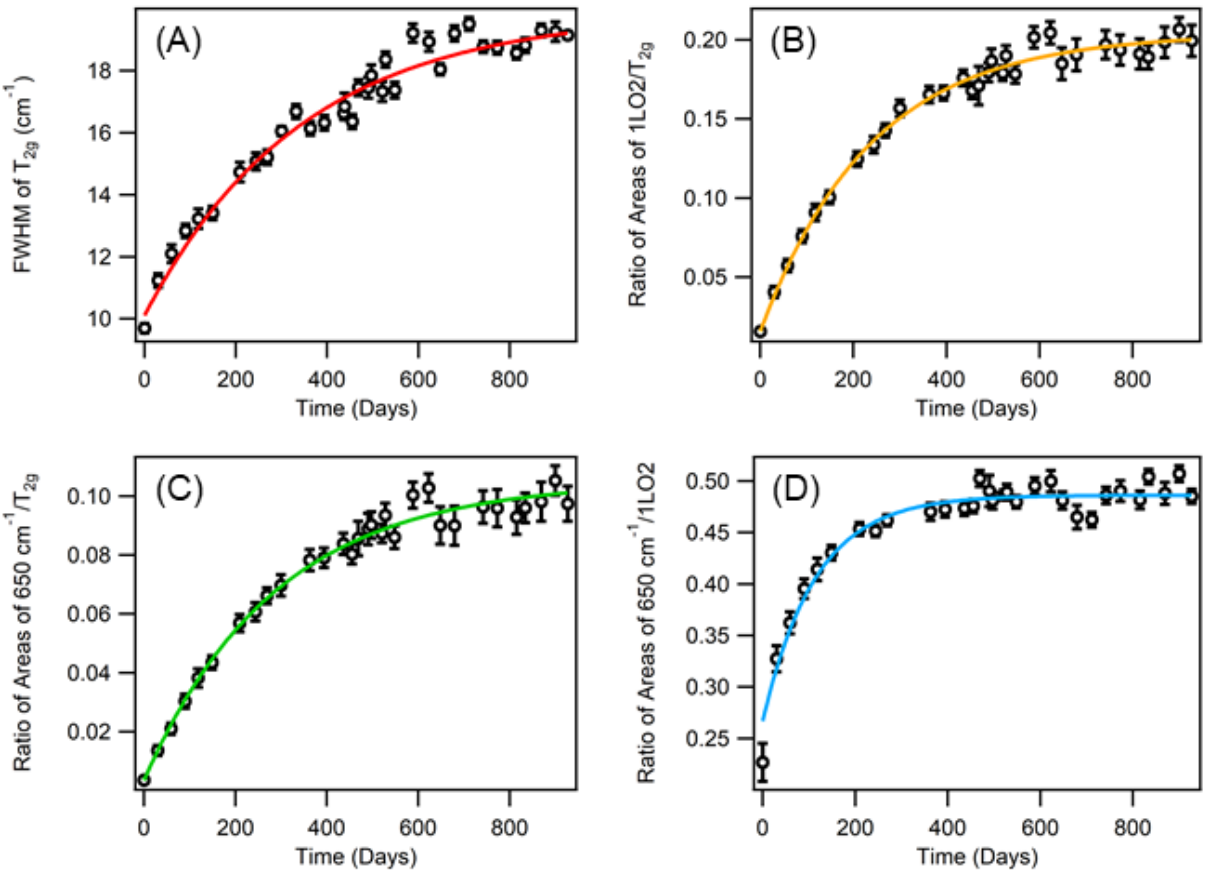

Fig. 4. Age dating curves for $^{240}PuO_2$ calcined at 1273 K of (A) FWHM of A, (B) ratio of areas of B/A, (C) ratio of areas of C/A and (D) ratio of areas of C/B. The error bars are estimated uncertainties at the 95% confidence interval.

The accumulated crystal lattice defects in a period of approximately 2 ½ years where the curve begins to plateau was responsible for doubling the FWHM of band A. Since the FWHM is inversely proportional to the phonon dephasing time, the phonon dephasing time was cut in half in this period. It is important to realize that most defects (~90%) produced by the alpha decay are self-annealed within 200 ns [2, 36]. In the case of B/A and C/A band ratios, the intensity of band A decreases with time while the intensity of the defect bands B and C grow with time. To put it in perspective, the relative intensity of band A between the aged and annealed material is approximately a factor of 4 to 10, dependent on the calcination temperature of the material. For material calcined at 1273 K the decrease in intensity is closer to a factor of 4. Therefore, it is expected that the intensity of the T_{2g} band for high fired calcined material aged for about 3 years ($^{240}PuO_2$) will decrease by a factor of 8 to 10 times from the original intensity. In contrast to the B/A and C/A bands ratios where the intensities are dependent on the growth of bands C and B and the intensity reduction of band A, the C/B ratio is a competition of defect formation. The C/B ratio shown in Figure 4D shows that the growth of band B started early in the aging process. Meanwhile, band C followed later and grew rapidly prior to a stabilization at a plateau level of ~0.5. It is important to understand that the intensities of bands B and C depends on the laser wavelength and the intensity of the band does not represent a necessarily a quantitative population since the ratio is wavelength dependent.

The lifetimes calculated from the FWHM of A, ratio of B/A, and ratio of C/A curves are 344, 238 and 287 days, respectively. Meanwhile, the age dating curves corresponding to the C/B curve has a much shorter lifetime of 113 days, suggesting that defects representing bands B and C have different origins in their formation. The curves representing the FWHM of A, ratio of B/A and ratio of C/A plateau at over 800 days for $^{240}PuO_2$. Meanwhile, the C/B curve plateaus at approximately 300 days of aging. These curves can be described by the exponential equation 1.

The ratio of C/B curve poses an interesting perspective on the defects of the material. The addition of impurities to a material, and the resulting damage to the crystal lattice, produces bands in the same location as the defect bands observed in materials with the fluorite structure. The work of Tanigushi *et al.* suggested that band B (D_1) in gadolinium-doped CeO_2 corresponds to O^{2-} vacancies [28]. Tanigushi *et al.* also indicated that band C corresponds to Ce in a different oxidation state (Ce^{3+}) for undoped CeO_2 and Gd^{3+} for doped CeO_2 where the metal atom is surrounded in an O^{2-} cube [28]. It is possible that in the case of PuO_2 a Pu^{3+} atom is within the O^{2-} cube allowing band C to grow. The oxygen vacancies are much easier to generate than the insertion of the metal ion in the cube. As time passes, an equilibrium is reached where the ratio of Pu metal atoms in the O_h octahedral symmetry to the O^{2-} vacancies remain constant.

Each metric as shown in the dating curves the FWHM of A, ratio of B/A, ratio of C/A and ratio of C/B have different physical origins which are affected by the crystallinity of the material and provides a different clock since last calcination. The band position in the spectrum is related to the bond force constant and the reduced mass via the equation $\upsilon = \sqrt{\frac{k}{m}}$. Damage to the crystal lattice results in bond weakening holding the atoms together. The weakening in the force constant leads to vibrational modes with lower energies. The FWHM of a band is related to the lifetime of the phonon. The shorter the lifetime, the broader the vibrational band corresponding to the optical phonon. Phonon lifetimes are shortened by the damage to the crystal lattice (traps). The intensity of the bands is inversely proportional to the FWHM since the band is spread over a significant number of energy levels therefore, as damage to the material occurs, the band FWHM becomes broader, the intensity is also expected to diminish. Finally, band intensity ratios or band area ratios can be used to understand how defects in the crystal are generated. The intensity/area of the defect bands emerging in the spectrum as the material ages are indicative of symmetry relaxation in the crystal or the formation of new chemical species. Correlation of material age from symmetry relaxation requires an anchor point which can be provided by the T_{2g} band. Band ratios can be used to understand the signatures related with crystal lattice damage and therefore age. Although the defect bands grow with time, the intensity of the T_{2g} band decreases with age. The ratio of areas of the defect band to the T_{2g} band provides a way to identify the PuO_2 since last calcination.

Calcination temperature used in the synthesis of PuO_2 from a Pu-bearing compound also affects the metrics (intensity, FWHM, band position and band ratios) in the spectrum. The calcination temperature and the calcination time are responsible for the material crystallinity [2, 3, 36]. Each calcination temperature converts a Pu-precursor compound (oxalate, fluoride, chloride, nitrate, etc.) into the oxide and crystallizes the material. The crystallinity of the material might not be complete at the calcination temperature. At high temperatures (>1173 K) where PuO_2 becomes a ceramic-like material and most defects in the crystal lattice are annealed, the Raman bands sharpen and shift to higher frequencies. Meanwhile, typical calcination temperatures of 723 and 923 K do not anneal

the crystal lattice in full. The crystal lattice defects measured through the FWHM and band intensity in the Raman spectrum suggest a material age older than expected [3]. A well calcined/annealed material will show a small defect band at best. After material calcination, the areas of the defect band/T_{2g} ratio is indicative of the crystallinity degree of the material. Separation of calcination temperature effects and aging effects can be accomplished by measuring the spectrum of the material of interest at different times. Age dating can be extracted through the removal of band features correlated with the calcination temperature.

The time dependent FWHM and band ratio data of the T_{2g} band and the defect bands in Figure 4 show very precise and accurate information of the $^{240}PuO_2$ material aging process. Four different curves were measured based on the FWHM and ratios of areas between the defect bands and T_{2g} band. These curves can be used for age dating the material since the fit is dependent only on the isotopic content of the material and the alpha decay rate of the different constituents. Although the curves shown in Figure 4 are related to $^{240}PuO_2$ calcined at 1273 K, the data can be normalized for any Pu isotope and to any calcination temperature. A methodology was developed to normalize the curves for any isotope and calcination material as shown in Figure 5. The high signal to noise ratio (S/N) for $^{240}PuO_2$ calcined at 1273 K with minimum crystal lattice defects and laser annealing resetting any aging effect requires a single point to provide age dating with an accuracy of just a month. In contrast to high fired PuO_2, lower calcination temperatures do not remove all the crystal lattice defects. The excess defects in the low-calcined material need to be accounted for to determine the material age. Since the alpha decay depends on the isotopic content, corrections are required to correct for age. Elemental analysis or gamma measurements might be required to determine the isotopes and abundance in the material. The alpha decay of $^{239}PuO_2$ is ~3.67 times slower than $^{240}PuO_2$. Therefore, the damage rate to the material from $^{239}PuO_2$ is reduced accordingly and the age determination is also increased proportionately. The age of the $^{239}PuO_2$ material can be estimated up to 10 years since last calcination by following the FWHM and the ratio of the areas of the bands. As mentioned before, the built-in defects due to incomplete annealing of the crystal and the resulting longer age can be corrected for by measuring the PuO_2 spectra at different times. Longer the times between the two measurements, the better to determine the age of the material. The S/N of the Raman spectra of PuO_2 materials calcined at lower temperatures may be low and introduce uncertainty into the age determination of the material. Figure 5B shows the concept for two-point age determination.

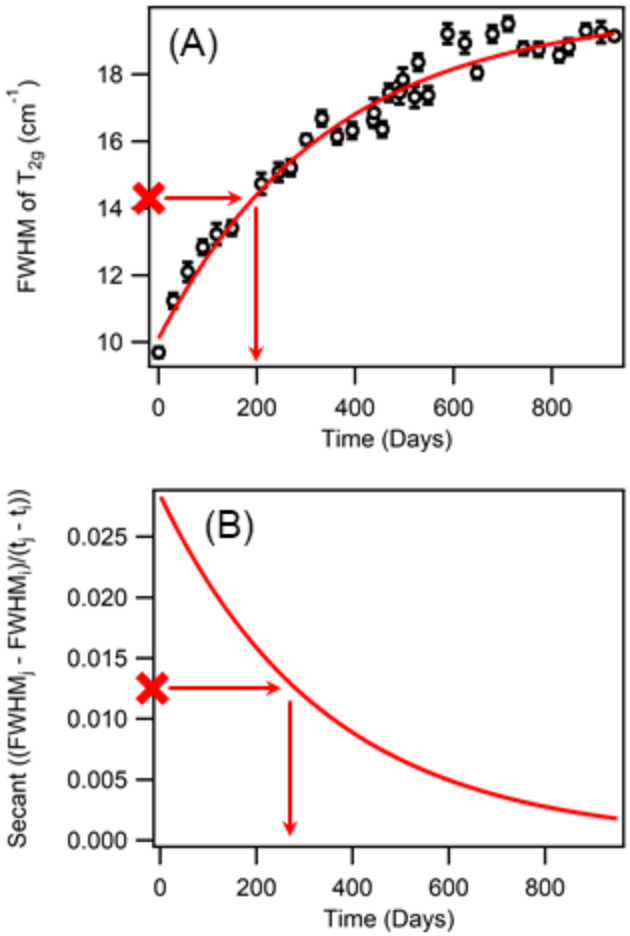

Fig. 5. Examples of age determination with FWHM of band A with (A) one data point if the sample is $^{240}PuO_2$ and (B) two data points for any other PuO_2 sample.

The secant is measured from two data points as shown in Figure 6, FWHM is shown as an example and can also be applied to the ratio of the areas of B/A, C/A and C/B. The secant is then used to determine the age of the material using equation 2.

$$age = \tau \cdot \ln\left(\frac{A}{secant}\right) + x_0 \qquad (2)$$

Where, τ is time constant for each measurement from the exponential fit to the calibration curves in Figure 4(A-D), A is maximum secant (slope) for the number of days from the fit to the calibration curve (equation 3), *secant* is measured as in Figure 6 (equation 4) and x_0 is the number of days between the two measurements. Equation 2 takes into account the data acquired at different times. The FWHM of band A or the areas of the band ratios can be used for age dating $^{240}PuO_2$, $^{239}PuO_2$ and any other PuO_2 isotope, as a proof-of-concept.

$$A = \frac{rise}{run} = \frac{\Delta y}{\Delta x} = \frac{\left(y_0 + A_0 \cdot \exp\left(-\frac{t}{\tau_0}\right)\right)_2 - \left(y_0 + A_0 \cdot \exp\left(-\frac{t}{\tau_0}\right)\right)_1}{t_2 - t_1} \qquad (3)$$

$$secant = \frac{rise}{run} = \frac{\Delta y}{\Delta x} = \frac{FWHM_2 - FWHM_1}{t_2 - t_1} \quad (4)$$

Where, y_0 is the maximum y value from the exponential fit to the calibration curves in Figure 4(A-D), A_0 is the y-intercept of the exponential fit to the calibration curves in Figure 4(A-D), τ_0 is the decay constant from the exponential fit to the calibration curves in Figure 4(A-D), t_1 and t_2 are number of days since calcination for measurement 1 and 2, respectively and $FWHM_1$ and $FWHM_2$ are the FWHM measured at t_1 and t_2, respectively, which can also be applied to the ratio of the areas of B/A, C/A and C/B.

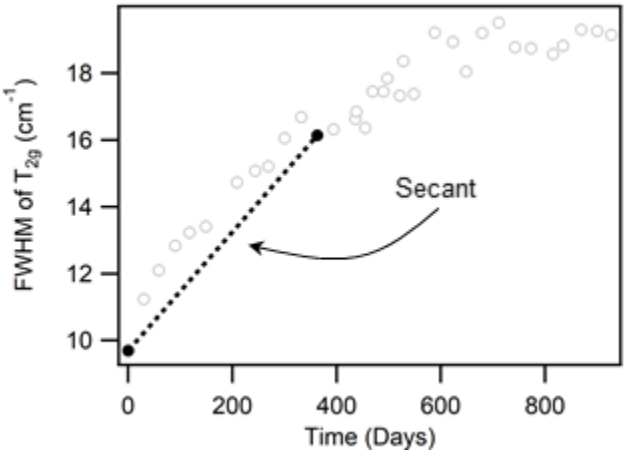

Fig. 6. Example secant fit of the FWHM of band A used for the methodology for age dating calculations. Methodology can also be applied to the ratio of the areas of B/A, C/A and C/B.

During this work, most of the data were acquired with $^{240}PuO_2$ calcined at 1273 K since a project is primarily funded for three to four years. Five spots of the $^{240}PuO_2$ sample were laser annealed. Non-annealed random spots on the same particle were also analyzed in this research. A comparison of predicted age for the laser annealed and random spots as compared to the actual age for the FWHM of band A is shown in Figure 7. The annealed spots and uncertainties are circled in Figure 7. Since the data shown in Figure 4 plateaus within the timeframe of these experiments, data collected within the first year for $^{240}PuO_2$ have high precision and accuracy due to the largest measurable changes in values. Data collected at times greater than 700 days show more scatter with higher uncertainty corresponding to the plateau region in Figure 4, and significant averaging will be required to improve the statistics.

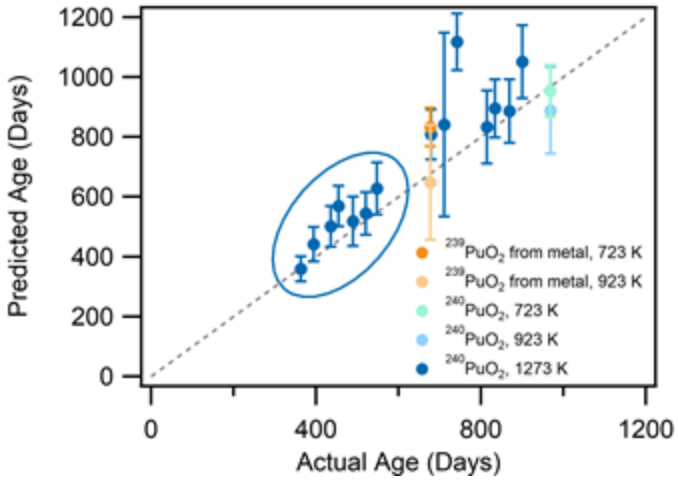

Fig. 7. Predicted age of PuO_2 samples from two measurements of the FWHM at the 95% confidence interval.

Few Raman spectra were recorded for $^{240}PuO_2$ calcined at 723 and 923 K and fewer spectra were recorded for $^{239}PuO_2$ from metal calcined at 723 and 923 K. These data were included as a proof-of-concept for this aging methodology. No data were measured for $^{239}PuO_2$ calcined at 1273 K, due to no sample availability.

Figure 8 shows the predicted age for different samples using the FWHM of band A and the three ratios of the fitted areas corresponding to the defects: B/A, C/A and C/B. The annealed spots have high precision and accuracy between the predicted age and the true age. Several samples with a known time since last calcination and samples produced from different precursors have been evaluated to understand the validity of the predicted age. The $^{239}PuO_2$ calcined at 723 and 923 K were synthesized from Pu metal.

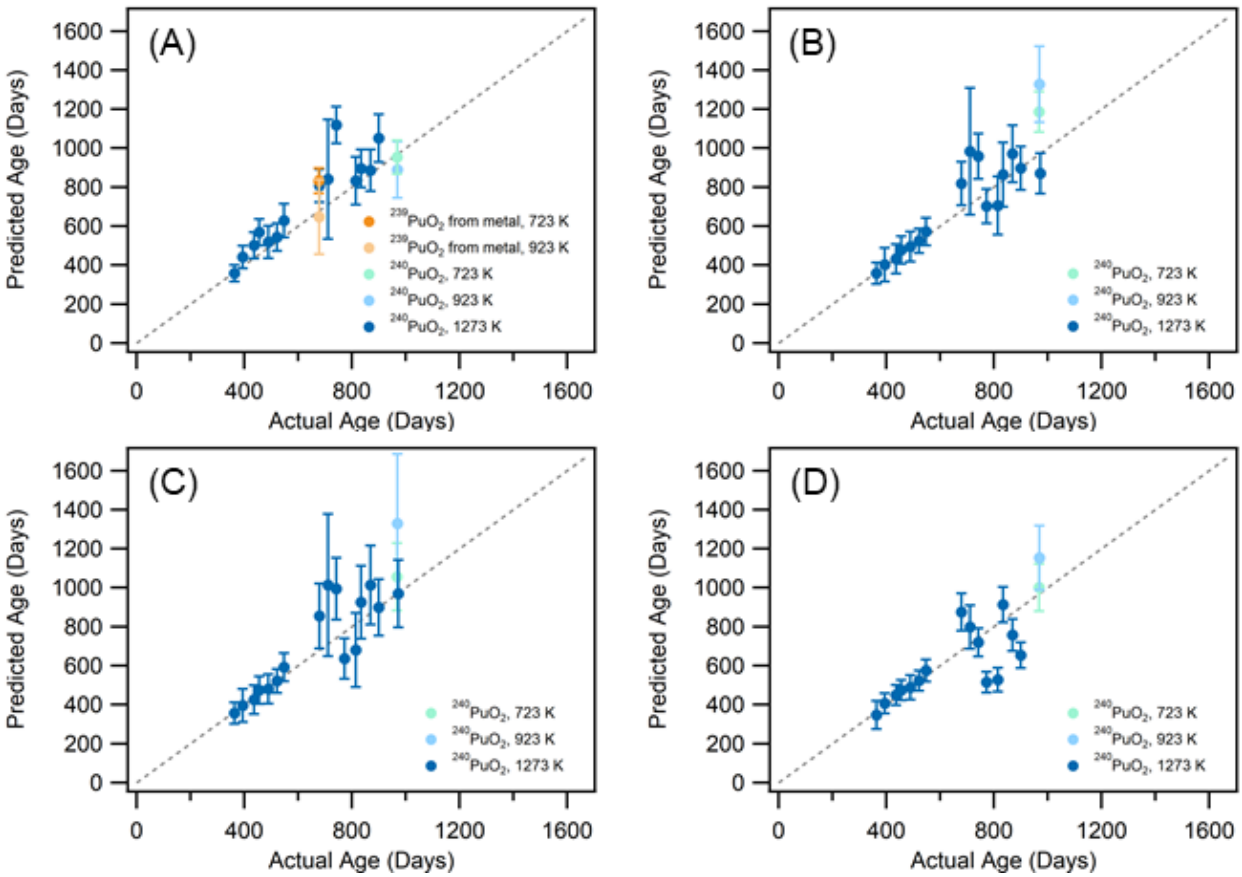

Fig. 8. Predicted age of samples from two measurements at the 95% confidence interval of (A) FWHM of A, (B) ratio of areas of B/A, (C) ratio of areas of C/A and (D) ratio of areas of C/B.

Comparison to Literature XRD Data

Figure 9 shows the relative changes in Raman spectral features as a function of storage time. The FWHM of the band corresponding to T_{2g} vibrational mode and ratio of the areas of the defect bands to T_{2g} peak is plotted against the exponential regressions of the change in the XRD lattice parameter as a function of storage time by Kato *et al.* with $^{238}PuO_2$, $^{239}PuO_2$ and a mixture of $^{239}PuO_2$, $^{238}PuO_2$ and $^{241}AmO_2$ [6]. Since the available XRD data was from different plutonium isotopes, the τ for ^{240}Pu was used to plot the exponential regressions on a common time scale. The error bars in Figure 9 are estimated uncertainties at the 95% confidence interval. The rise and shape of curves from the changes in the Raman spectral figures in Figure 9 were found to be similar and match well to the curves observed with XRD.

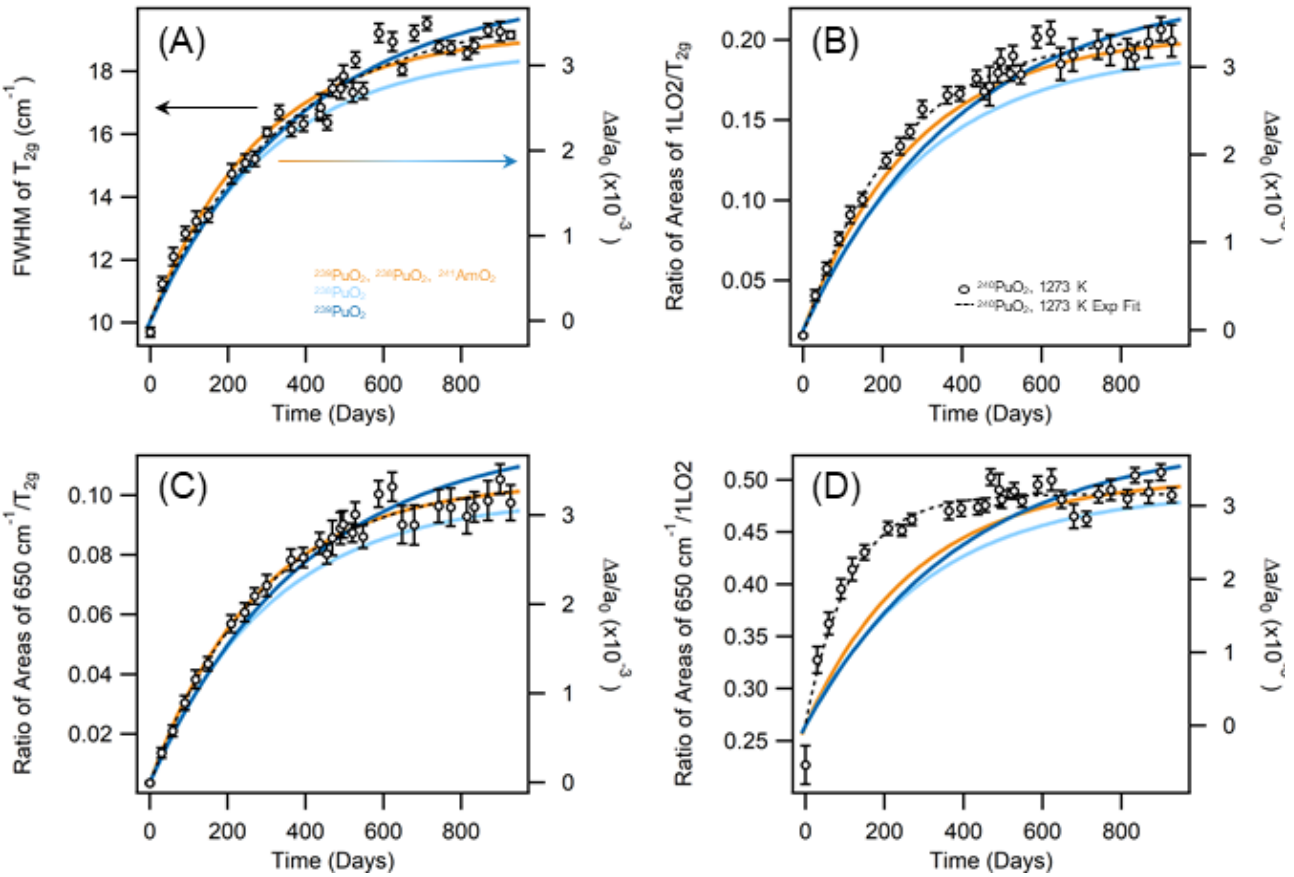

Fig. 9. Relative changes in the Raman spectral features as a function of time (A) FWHM of A, (B) ratio of areas of B/A, (C) ratio of areas of C/A and (D) ratio of areas of C/B. The error bars are estimated uncertainties at the 95% confidence interval. The colored curves correspond to extrapolations based on prior XRD measurements, (orange line) mixture of $^{239}PuO_2$, $^{238}PuO_2$ and $^{241}AmO_2$, (light blue line) $^{238}PuO_2$ and (dark blue line) $^{239}PuO_2$, to plot the exponential regressions on a common time scale the decay constant (τ) for ^{240}Pu was used [6].

The number density of damage sites depends on elapsed time, but also on the inventory of alpha-emitters within the material. Consistent with the damage in previously studied nuclear materials, XRD measurements of the PuO_2 lattice parameter show an increase as a function of storage time due to self-radiation damage from alpha-decay of plutonium. Equation 1 represents the established relationship. The established relationship is dependent on three different constants: τ (decay constant associated with the alpha-emitting isotope(s) present), A (maximum change in lattice parameter), and B (a measure of the rate of change of the lattice parameter, kinetic constant). A and B are intrinsic to the PuO_2 lattice and will be the same for different isotopes of plutonium. Because τ is different for each plutonium isotope, using the same τ to plot the exponential regressions for each isotope places all the regressions onto the same time scale, allowing for direct comparisons.

The Raman results from the measured FWHM of the T_{2g} band as a function of storage time match the lattice parameter change measured with XRD (Figure 9A). The ratio of the fit areas of the aging bands and T_{2g} bands with respect to storage time also matches the XRD results (Figure 9B and C). The ratio of the fit areas of the aging bands decayed faster than the XRD results (Figure 9D). These

Raman results indicate an exponential relationship with storage time, analogous to the XRD literature results and our results are also consistent with alpha-recoil track studies performed on other nuclear materials. The data strongly suggest that the results obtained from Raman spectroscopy follow very closely the results on the expansion of the lattice constant with XRD indicating that both measurements are highly correlated.

Summary

The monthly temporal evolution of the T_{2g} band and the growth of the defect bands was followed for five laser-annealed spots of a $^{240}PuO_2$ sample calcined at 1273 K using Raman spectroscopy for several years. The FWHM, band intensity and position for the T_{2g} band and the defect band intensity were the focus of this investigation. In this study, the FWHM of the T_{2g} band, and the ratios of the areas of bands B/A, C/A, and C/B was measured. In addition to the $^{240}PuO_2$ sample, a limited number of data points were acquired from $^{239}PuO_2$ samples synthesized from Pu metal and calcined at 723 and 923 K. The temporal data was modeled, and the fitted exponential curve was similar to the lattice constant expansion curve measured with XRD. The data show that the spectral features accurately measures the time since a PuO_2 sample was calcined, based on the growth of alpha-induced crystalline defects. This method of age-dating produces results that agree with XRD measurements when applied to bulk lattice analysis. This Raman spectroscopy method can be used to measure self-radiation damage from alpha-decay of plutonium that matches literature XRD results with only a 10 μm sample.

Acknowledgements

This work was funded by the Office of Defense Nuclear Nonproliferation Research and Development within the U.S. Department of Energy's National Nuclear Security Administration under project SR19-Spec-Signatures NDD3Bb. This manuscript was authored by Savannah River Nuclear Solutions, LLC under Contract No. DE-AC09-08SR22470 with the U.S. Department of Energy. The United States Government retains and the publisher, by accepting this article for publication, acknowledges that the United States Government retains a non-exclusive, paid-up, irrevocable, worldwide license to publish or reproduce the published form of this work, or allow others to do so, for United States Government purposes.

References

[1] M.J. Sarsfield, R.J. Taylor, C. Puxley, H.M. Steele, Raman spectroscopy of plutonium dioxide and related materials, J. Nucl. Mater. 427(1–3) (2012) 333-342.

[2] W.G. Wolfer, Radiation effects in plutonium, Los Alamos Sci. 26 (2000) 274-285.

[3] E. Villa-Aleman, N.J. Bridges, T.C. Shehee, A.L. Houk, Raman microspectroscopy of PuO_2 particulate aggregates, J. Nucl. Mater. 515 (2019) 140-149.

[4] E. Villa-Aleman, A.L. Houk, N.J. Bridges, T.C. Shehee, Raman spectroscopy: A tool to investigate alpha decay damage in a PuO2 crystal lattice and determining sample age since calcination, J. Raman Spectrosc. 50(6) (2019) 899-901.

[5] D. Staicu, T. Wiss, V.V. Rondinella, J.P. Hiernaut, R.J.M. Konings, C. Ronchi, Impact of auto-irradiation on the thermophysical properties of oxide nuclear reactor fuels, J. Nucl. Mater. 397(1) (2010) 8-18.

[6] M. Kato, A. Komeno, H. Uno, H. Sugata, N. Nakae, K. Konashi, M. Kashimura, Self-radiation damage in plutonium and uranium mixed dioxide, J. Nucl. Mater. 393(1) (2009) 134-140.

[7] R.M. Harker, C. Puxley, Development of point defect Raman signatures in PuO_2 through self-irradiation, in: R. Caciuffo (Ed.) Plutonium Futures - The Science 2016, Baden-Baden, Germany, 2016, pp. 62-65.

[8] M.H. Rand, A.C. Fox, R.S. Street, Radiation Self-Damage in Plutonium Compounds, Nature 195(4841) (1962) 567-568.

[9] K. Mendelssohn, E. King, J.A. Lee, M.H. Rand, C.S. Griffin, R.S. Street, Plutonium 1965, Chapman and Hall, London, 1967.

[10] W.C. Mosley, Self-Radiation Damage in Curium-244 Oxide and Aluminate, J. Am. Ceram. Soc. 54(10) (1971) 475-479.

[11] M. Noe, J. Fuger, Self-radiation effects on the lattice parameter of 238PuO2, Inorg. Nucl. Chem. Lett. 10(1) (1974) 7-19.

[12] C. Hurtgen, J. Fuger, Self-irradiation effects in americium oxides, Inorg. Nucl. Chem. Lett. 13(3) (1977) 179-188.

[13] H.E. Schmidt, J. Richter, H. Matzke, J. van Geel, The Effect of Self-Irradiation on the Thermal Conductivity of Plutonium and Americium Oxides, Proceedings of the 22nd International Conference on Thermal Conductivity, 1994, pp. 920-928.

[14] E.T. Peskie, A.Q. Loveless, T.G. Schaaff, H.L. Hall, Radiation Damage as a Possible Metal Chronometer for Pre-Detonation Nuclear Forensics, Int. J. Nucl. Secur. 1(1) (2015) 1-11.

[15] A.M. Loveless, T.G. Schaaff, A.L. Garner, Age-dating uranium metal using microstructural damage, Ann. Nucl. Energy 83 (2015) 298-301.

[16] G.M. Begun, R.G. Haire, W.R. Wilmarth, J.R. Peterson, Raman spectra of some actinide dioxides and of EuF_2, J. Less-Common Met. 162(1) (1990) 129-133.

[17] J.R. Schoonover, F. Weesner, G.J. Havrilla, M. Sparrow, P. Treado, Integration of elemental and molecular imaging to characterize heterogeneous inorganic materials, Appl. Spectrosc. 52(12) (1998) 1505-1514.

[18] C. Jégou, R. Caraballo, S. Peuget, D. Roudil, L. Desgranges, M. Magnin, Raman spectroscopy characterization of actinide oxides $(U_{1-y}Pu_y)O_2$: Resistance to oxidation by the laser beam and examination of defects, J. Nucl. Mater. 405(3) (2010) 235-243.

[19] D. Hudry, C. Apostolidis, O. Walter, A. Janßen, D. Manara, J.-C. Griveau, E. Colineau, T. Vitova, T. Prüßmann, D. Wang, C. Kübel, D. Meyer, Ultra-small plutonium oxide nanocrystals: An innovative material in plutonium science, Chem. - Eur. J. 20(33) (2014) 10431-10438.

[20] R. Mohun, L. Desgranges, J. Léchelle, P. Simon, G. Guimbretière, A. Canizarès, F. Duval, C. Jegou, M. Magnin, N. Clavier, N. Dacheux, C. Valot, R. Vauchy, Charged defects during alpha-irradiation of actinide oxides as revealed by Raman and luminescence spectroscopy, Nucl. Instrum. Methods Phys. Res., Sect. B 374 (2016) 67-70.
[21] M. Naji, N. Magnani, L.J. Bonales, S. Mastromarino, J.Y. Colle, J. Cobos, D. Manara, Raman spectrum of plutonium dioxide: Vibrational and crystal field modes, Phys. Rev. B 95(10) (2017) 104307.
[22] D. Manara, M. Naji, S. Mastromarino, J.M. Elorrieta, N. Magnani, L. Martel, J.Y. Colle, The Raman fingerprint of plutonium dioxide: Some example applications for the detection of PuO_2 in host matrices, J. Nucl. Mater. 499 (2018) 268-271.
[23] L. Morales, The Path of PuO_{2+x}, in: N.M. Technology (Ed.) Los Alamos National Laboratory, Los Alamos National Laboratory, 2004, pp. 3-8.
[24] C. Madic, G.M. Begun, D.E. Hobart, R.L. Hahn, Raman spectroscopy of neptunyl and plutonyl ions in aqueous solution: hydrolysis of neptunium(VI) and plutonium(VI) and disproportionation of plutonium(V), Inorg. Chem. 23(13) (1984) 1914-1921.
[25] G. Guimbretière, L. Desgranges, C. Jegou, A. Canizarès, P. Simon, R. Caraballo, N. Raimboux, M.F. Barthe, M.R. Ammar, O.A. Maslova, F. Duval, R. Omnée, Characterization of nuclear materials in extreme conditions: Raman spectroscopy approach, IEEE Trans. Nucl. Sci. 61(4) (2014) 2045-2051.
[26] A.J. Schwartz, M.A. Wall, T.G. Zocco, W.G. Wolfer, Characterization and modelling of helium bubbles in self-irradiated plutonium alloys, Philos. Mag. 85(4-7) (2005) 479-488.
[27] A. Nakajima, A. Yoshihara, M. Ishigame, Defect-induced Raman spectra in doped CeO_2, Phys. Rev. B 50(18) (1994) 13297-13307.
[28] T. Taniguchi, T. Watanabe, N. Sugiyama, A.K. Subramani, H. Wagata, N. Matsushita, M. Yoshimura, Identifying Defects in Ceria-Based Nanocrystals by UV Resonance Raman Spectroscopy, J. Phys. Chem. C 113(46) (2009) 19789-19793.
[29] E. Villa-Aleman, A.L. Houk, D.D. Dick, S.E. Hunyadi Murph, Hyper-Raman spectroscopy of CeO_2, J. Raman Spectrosc. 51(7) (2020) 1260-1263.
[30] J.D. Axe, G.D. Pettit, Infrared Dielectric Dispersion and Lattice Dynamics of Uranium Dioxide and Thorium Dioxide, Phys. Rev. 151(2) (1966) 676-680.
[31] L. Manes, A. Barisich, Dielectric Response and Infrared Spectrum of Stoichiometric Plutonium Dioxide by Optical Reflection and Absorption Spectroscopy, Phys. Stat. Sol. (A) 3(4) (1970) 971-981.
[32] M. Naji, N. Magnani, J.Y. Colle, O. Beneš, S. Stohr, R. Caciuffo, R.J.M. Konings, D. Manara, Raman Scattering from Decoupled Phonon and Electron States in NpO_2, J. Phys. Chem. C 120(9) (2016) 4799-4805.
[33] L.J. Bonales, J.M. Elorrieta, Á. Lobato, J. Cobos, Raman Spectroscopy, a Useful Tool to Study Nuclear Materials, in: M.T. Stauffer (Ed.) Applications of Molecular Spectroscopy to Current Research in the Chemical and Biological Sciences, IntechOpen, 2016.
[34] J.-M. Costantini, S. Miro, G. Gutierrez, K. Yasuda, S. Takaki, N. Ishikawa, M. Toulemonde, Raman spectroscopy study of damage induced in cerium dioxide by swift heavy ion irradiations, J. Appl. Phys. 122(20) (2017) 205901.
[35] J. Schoenes, Electronic transitions, crystal field effects and phonons in UO_2, Phys. Rep. 63(6) (1980) 301-336.

[36] D.L. Clark, S.S. Hecker, G.D. Jarvinen, M.P. Neu, Plutonium, in: L.R. Morss, N.M. Edelstein, J. Fuger (Eds.), The Chemistry of the Actinide and Transactinide Elements, Springer Netherlands, Dordrecht, 2011, pp. 813-1264.